Materials Science & Engineering A 776 (2020) 139038

Contents lists available at ScienceDirect

Materials Science & Engineering A

journal homepage: www.elsevier.com/locate/msea

Critical compressive strain and interfacial damage evolution of EB-PVD thermal barrier coating

Fulei Jing [a], Junjie Yang [b,*], Zhengmao Yang [c,*], Wu Zeng [d]

[a] Aero Engine Academy of China, Aero Engine (Group) Corporation of China, Beijing, China
[b] Institute for Aero engine, Tsinghua University, Beijing, China
[c] Institute of Mechanics, Chinese Academy of Sciences, Beijing, China
[d] School of Aerospace Engineering, Tsinghua University, Beijing, China

ARTICLE INFO

Keywords:
Thermal barrier coating
Critical compressive strain
Interfacial damage evolution
Isothermal and cyclic oxidation
Life prediction

ABSTRACT

The durability evaluation of electron beam physical vapor deposited (EB-PVD) thermal barrier coating (TBC) systems is one of the critical issues in engineering applications. The interfacial toughness degradation as a function of the thickness of thermally grown oxide (TGO) was investigated through isothermal oxidation and cyclic oxidation tests for single-crystal superalloy specimens with an EB-PVD TBC. The critical strain criterion of TBC compression spalling was proposed through compression tests at room temperature according to noncontact full-field strain measurement technology and the digital image correlation (DIC) method. Based on a simplified mechanical model of TBC systems and elastic buckling theory, the interfacial damage was described by the critical compressive strain at spallation considering residual stress in the ceramic top coat (TC). The results indicated that the damage induced by cyclic oxidation is greater than that induced by isothermal oxidation at the same TGO thickness, showing additional damage induced in thermal cycles. Then, a new TBC life prediction model based on the nonlinear accumulation of oxidation damage and cyclic damage was developed, and the error between the damage prediction and the testing results was found to be no more than ±10%.

1. Introduction

Electron beam physical vapor deposited (EB-PVD) thermal barrier coatings (TBCs) are widely used in air-cooled turbine blades of advanced aeroengines to provide thermal and oxidation protection between the blade substrate superalloy and high-temperature gas [1,2], extending the blade life by reducing the in-service temperature of the substrate superalloy and effectively improving aeroengine performance through increasing gas temperature at the turbine inlet or reducing the mass flow of cooling air in the turbine [3,4].

A typical EB-PVD TBC system consists of a ceramic top coat (TC) with a columnar crystal microstructure to provide strain tolerance and an oxidation-resistant aluminum-rich metal bond coat (BC). In a high-temperature environment, a thin layer of thermally grown oxide (TGO) at the ceramic–metal interface formed due to elements such as Al in the BC reacting with oxygen passing through the TC [5,6], in which the main component is α-Al_2O_3, is usually dense.

TGO can play an antioxidative role by preventing further penetration of oxygen. However, the thermal expansion coefficient of TGO is less than that of the adjacent TC and BC, resulting in a thermal mismatch in the in-plane direction in each layer of the TBC system during service [7–9]. Once the TBC is peeled off, the blade substrate superalloy is directly exposed to the high-temperature gas environment, which exceeds the temperature the material can withstand, further resulting in the ablation of blades and even fracture. Therefore, the accurate evaluation of durability under in-service loading is one of the key issues faced by TBC applications.

In general, experiments show that the spalling process of TBC systems consists of four stages [10–12]: (i) ceramic–metal interface damage; (ii) delamination from existing defects or damaged areas; (iii) TC buckling; and (iv) macroscopic spalling. The whole failure process, from the initial damage to the final failure, involves multiple scales in time and space. For damage evolution and interfacial delaminations, the time may range from a few minutes to hundreds of hours, while buckling and spalling are processes of transient instability for which the time scale is usually 10^{-1} s. The damage of TBC systems initiates from the ceramic–metal interface, necessitating microscopic analysis of approximately several micrometers, and then the damage accumulation causes the TBC system to delaminate on the order of tens of micrometers to 1 millimeter, until final peeling from 1 millimeter to several

* Corresponding authors.
E-mail addresses: yangjunjie@tsinghua.edu.cn (J. Yang), zmyang@imech.ac.cn (Z. Yang).

https://doi.org/10.1016/j.msea.2020.139038
Received 19 December 2019; Received in revised form 21 January 2020; Accepted 31 January 2020
Available online 3 February 2020

centimeters [13]. The complexity of scales in time and space makes it difficult to accurately assess the damage and spalling process of TBCs.

At present, phenomenological models based on the competition mechanism between oxidation-driven failure and mechanical-driven failure has been widely used to predict the life of TBC systems, it is assumed that the damage depends on the ratio of the internal effective strain to the failure strain and that the effect of oxidation on the damage is described by reducing the failure strain [14]. For the EB-PVD TBC system, the effective strain can generally take the in-plane maximum tensile strain, the range of in-plane inelastic strain, the range of in-plane mechanical strain [15] in the TGO and the range of out-of-plane stress [16] at the interface of the TGO-BC and so on. The failure strain is defined as the strain corresponding to the spalling of TBCs only experienced one thermal cycle, and it decreases with increasing TGO thickness. In essence, such models idealize the growth of TGO into a quasistatic thickness growth process, and the damage of TBC under the specific TGO thickness is calculated through analyzing the mechanical behavior of each layer using the macroscopic simplified mechanical model or the microscopic finite element model. Therefore, the local crack initiation life is obtained through the linear accumulated damage method.

However, some experiments [16] show that the TC may remain adhered even if there are local cracks near the TGO, making these models difficult to be effectively supported and verified. In addition, the damage caused by thermal cycling in the models can be evaluated only by the TBC spontaneous spalling life corresponding to an effective cumulative damage of 1, whereas the evolution of the damage during the process cannot be verified due to lack of experimental data, resulting in the limitation of prediction accuracy and the applicability of models.

The macroscopic spalling of the TBC usually occurs in the cooling stage, which is caused by compression loading on the TC, leading to large-scale buckling. The driving force is identified as the in-plane compressive stress due to the thermal mismatch, and the resistance is the toughness of the ceramic–metal interface [10,11]. The interface damage of the TBC system during service, such as local micro cracks and defects, reduces the effective bearing area of the ceramic–metal interface, resulting in a decrease in the interface toughness and load-carrying capacity. Based on the above viewpoints, Courcier et al. [13] assumed that the interface damage of the TBC system undergoing different thermal loading states was proportional to the decrease in the interface toughness relative to the prepared state, and the interface toughness was uniformly characterized through the TBC compression spalling test at room temperature. Then, the relationship between the measured damage and the TGO thickness and the mechanical behavior of the BC was then established. Thus, a life model of the TBC based on the interface damage was formed. The method considers the cross-scale correlation between the TBC macroscopic spalling and the interface microscopic damage and quantitatively describes the evolution of the interface damage, improving the prediction accuracy of the damage model. However, there are still some issues that have not yet been solved. For example, the visual determination of the critical compressive strain of TBC spalling relies on stochastic processes [17], and it is difficult to directly measure the spalling strain using the extensometer for nonuniform-cross-section specimens. In addition, the adhesion of the strain gauge changes the stiffness of the TBC thus affecting the spalling. Moreover, the influence of the residual stress induced by the TBC preparation process on the buckling of the TC is not explicitly considered.

In present work, based on the noncontact full-field strain measurement [18] and the digital image correlation (DIC), a new criterion for TBC spalling initiation is proposed through the compression spalling test at room temperature with EB-PVD TBC specimens undergoing different isothermal oxidation times and the number of thermal cycles, and then the critical spalling compression strain of TBCs is accurately identified. Considering the influence of the residual stress in TC on the elastic bulking, an interface damage model of the TBC system is modified, and an evolution equation of interface damage is constructed based on the relationship between the measured damage and the TGO thickness and thermal cycles and is preliminarily verified through the existing experimental data. Moreover, a nonlinear accumulation damage model of the TBC based on the interface damage presented can accurately predict the spalling life of the TBC system.

Table 1
Target materials chemical composition (wt pct.).

Ni	Cr	Al	Y	Si	Cu	Fe
Bal.	15–20	10–15	0.2–1.0	0.6–1.2	≤0.05	≤0.5

Table 2
PWA1484 chemical composition (wt pct.).

Ni	Co	Cr	Mo	W	Ta	Re	Ti	Al	C
Bal.	10	5	1.7	6	8.5	3	1	5.5	0.02

2. Materials and experiments

2.1. Materials description

Electron beam physical vapor deposited (EB-PVD) ceramic top-coat was deposited on the PWA1484 single crystal superalloy substrate. The TC material is 8YSZ (8% Y_2O_3+ZrO_2) with a thickness of not less than 100 μm, and the BC is NiCrAlYSi with a thickness of not less than 30 μm. The chemical compositions of the target materials are given in Table 1. The average grain size is no greater than 30 μm.

The PWA1484 is a second-generation nickel-based single crystal superalloy, whose composition is given in Table 2. Cylindrical test specimens having a common geometry for both tests were machined from the plates of PWA1484 having the dimensions shown in Fig. 1(a). In addition, to avoid the TBC peeling off from the edge of specimens during the compression process [16], hourglass specimens are used. The Scanning electron microscope (SEM, JSM-7001F, Japan) morphology of the TBC system is shown in Fig. 1(b), revealing that the TC has a columnar structure.

TBC systems are processed by the EB-PVD method as follows:

Step 1 Cleaning the substrate by wet sandblasting with corundum particles with a diameter between 100 μm and 125 μm under 0.2 MPa air;

Step 2 Depositing the material NiCrAlYSi of the BC on the specimen;

Step 3 Heating the specimen with BC at 1000 °C for 4 h in vacuum;

Step 4 Shot-peening is performed by using the glass pills with a diameter between 150 μm and 300 μm under 0.3 MPa air to obtain uniform roughness;

Step 5 Heating the specimen at 1000 °C for 2 h in vacuum;

Step 6 Repeating step 1;

Step 7 Depositing the ceramic material 8YSZ of the TC;

Step 8 Checking the specimens; TBC is considered to be acceptable when the procession control panels are bent at 90° without TBC peeling.

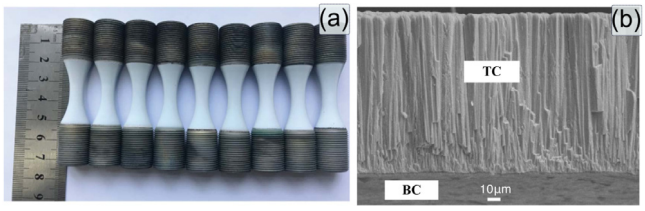

Fig. 1. EB-PVD TBC system. (a) Specimens with the EB-PVD TBC, and (b) SEM morphology of the EB-PVD TBC system.

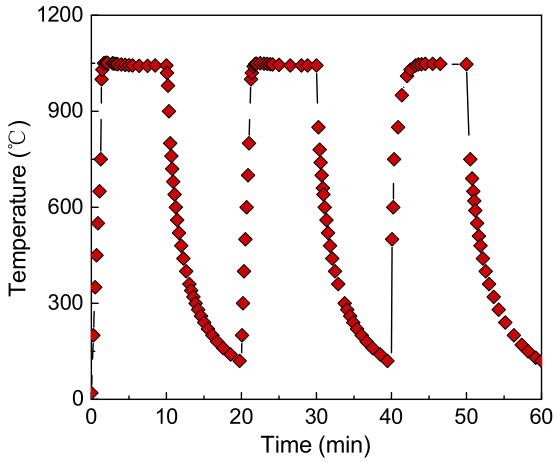

Fig. 2. Temperature change with time in the cyclic oxidation tests.

2.2. Experimental procedure

The qualified EB-PVD TBC specimens were divided into two groups that were either subjected to isothermal oxidation loadings or subjected to cyclic oxidation loadings. Through the QSX1600 muffle furnace, the isothermal oxidation test was performed at a constant temperature of 1050 °C, and the cyclic oxidation test was conducted using a 20-min thermal cycle with a maximum temperature of 1050 °C, including heating for 10 min, followed by then air cooling for 10 min. The typical thermal cycle is shown in Fig. 2, and the details of the thermal cyclic tests can refer to the previous work [19].

After undergoing different isothermal oxidation times or numbers of thermal cycles, the EB-PVD TBC specimens were removed and cooled to room temperature for the compression test to investigate the ceramic–metal interfacial toughness. The key to the issue is to acquire the critical strain of TBC compression spalling accurately. However, the macroscopic spalling of the TBC due to the buckling of the TC is a transient process with a time scale of a fraction of a second. Therefore, the conventional method of visually determining the compressive critical strain is arbitrary and has strong errors. In addition, the strain concentration zone generally occurs in the gauge section because of the nonuniform cross-section of the hourglass specimens, which makes it is difficult to directly measure the TBC peeling strain with the extensometer. Moreover, since the TBC is very thin, the adhesion of the strain gauge can profoundly change the TC stiffness, thus affecting the TBC spalling process. Therefore, the DIC-based noncontact full-field strain measurement technology is adopted herein to accurately obtain the strain evolution of the TBC surface with loading time.

A 3D noncontact full-field strain measurement system was used to measure the surface strain of specimens, and the noncorrosive speckles were sprayed on the surface of specimens. Then, the compression tests were carried out at room temperature using a servo-hydraulic axial/torsion material testing machine (MTS, 809, USA) at an axial displacement rate of 0.001 mm/s. The test is terminated when the TBC is peeled off from the specimen. Because the real-time displacement of the specimen surface is obtained based on the binocular vision principle and the DIC method [18,20,21], the evolution of strain distribution can be calculated, as shown in Fig. 3.

Although there are residual strains in the TBC system without loading due to the processes and the difference in the thermal expansion coefficient of each layer, the initial surface strain of the TBC can be calibrated to zero by the digital image correlation (DIC, VIC-3D SR-9M, USA), as shown in the picture at 0 s in Fig. 3. In addition, the influence of residual strains is considered in the damage equation mentioned later. Then, as the specimen is subjected to a linearly increasing axial compressive load, the strain concentration zone gradually appears in the middle of the specimen, and its shape remains stable during loading, as shown in the pictures at 30 s~150 s in Fig. 3. The strain concentration zone exhibits a certain angle with respect to the axis of the specimen, which is caused by the orientation angle deviation of the single-crystal substrate [22]. As the compression load is further increased, the strain concentration zone is abruptly converted into a thin strip, as shown in the picture at 180 s in Fig. 3. It can be observed that the strain gradient at the edge of the zone is significantly increased, and then TBC macroscopic spalling occurs at 190 s. Note that the shape of the spalling zone is substantially consistent with the strip of the strain concentration zone, as shown in Fig. 4.

3. Results and analysis

3.1. Critical strain of compression spalling at room temperature

During the compression test at room temperature, the TBC showed a significant strain concentration in the middle of the specimens before macroscopic spalling, as shown in Fig. 3. Five points numbered P0 ~ P4 are selected in the spallation zone, including the point of the maximum absolute value of compressive strain. The second principal strain on the surface, i.e., the surface compression strain, is extracted, and its evolution with the loading time is shown in Fig. 5.

Note that there is a significant slope change in the second principal strain of the surface. Considering that the displacement rate of the test machine remains constant, the reason for the sudden change in the second principal strain on the surface may come from two aspects: (i) the deformation of the TBC is inconsistent with that of the substrate alloy because of the delamination in the TBC system and (ii) the plastic deformation of the single-crystal substrate.

In comparison with the test machine pressure curve in Fig. 6, the compressive force remains linear for a period of time after the second principal strain slope on the surface is abrupt; that is, the substrate superalloy does not yield significant plastic deformation, thereby implying that the sudden change in the surface second principal strain is caused by the delamination and bulging of the TBC. Therefore, the abrupt change in slope of the surface second principal strain can be considered as the criterion for the spalling initiation of the TBC herein, and the maximum compressive strain in the spalling zone corresponding to this position is defined as the critical strain. Fig. 6 shows that the evolution of the second principal strain at each point of the TBC spalling zone is approximately bilinear. Therefore, the corresponding curve can be fitted with a piecewise linear function, and then the intersection of the two lines is obtained as the inflection point of the slope, corresponding to the critical strain, ε_{crit}. Thus, the evolution of the critical strain with isothermal oxidation time and the number of thermal cycles can be obtained, as shown in Fig. 7. It can be observed that the critical strain reaches zero after about 120h of isothermal oxidation, as well as after 1200 cycles of cyclic oxidation, which means that the TBC spontaneously spalls after undergoing only thermal oxidation.

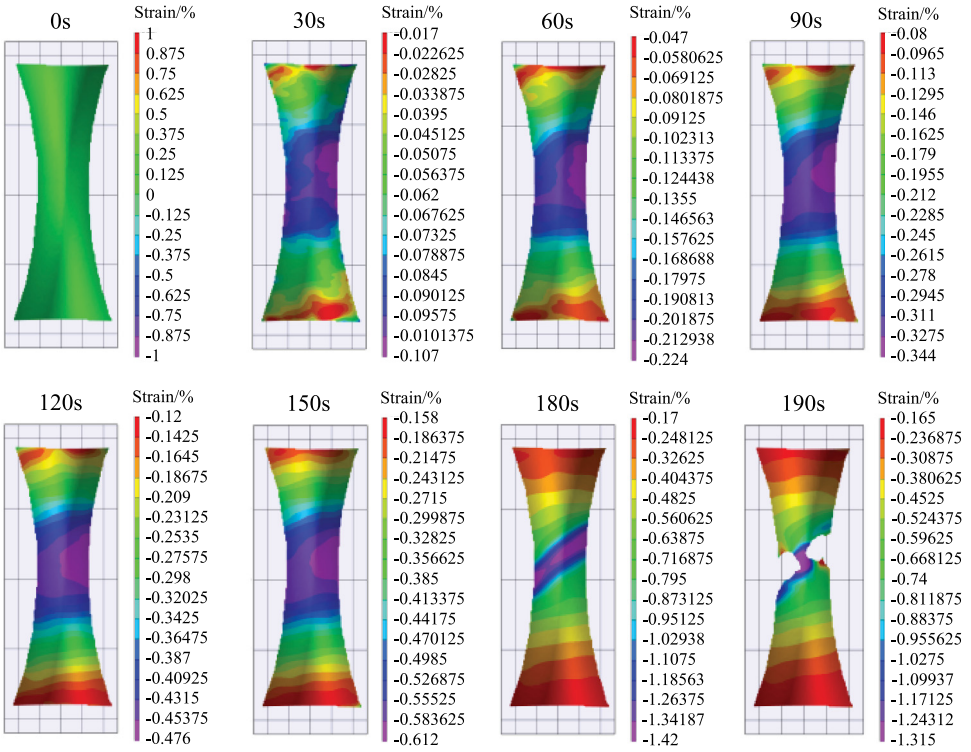

Fig. 3. Evolution of the TBC surface strain distribution obtained by DIC during the compression test.

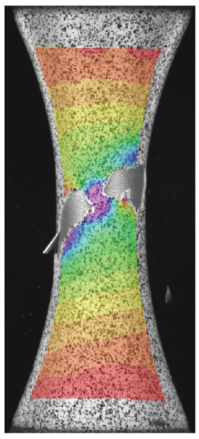

Fig. 4. The TBC spalling zone and the strain distribution measured by DIC.

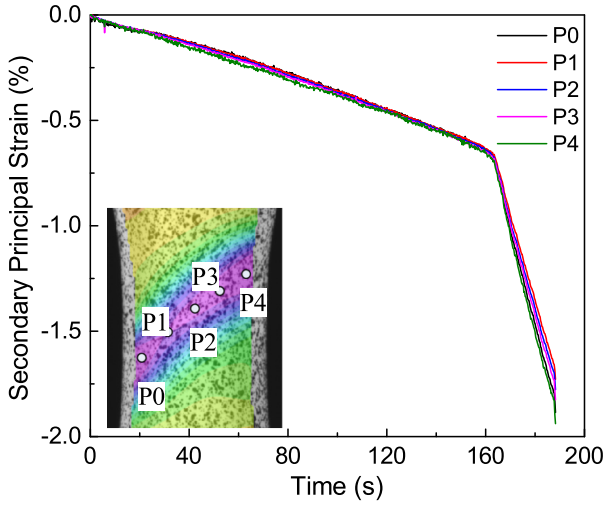

Fig. 5. Evolution of the TBC surface secondary principal strain in the spallation area.

3.2. Thickness of TGO

TGO is considered to be the critical component restricting the service life of TBCs [6–9]. Fig. 8 shows the typical interface morphology between the ceramic and metal for the specimen undergoing thermal oxidation, as observed by SEM. In a comparison with the initial interface morphology shown in Fig. 1, the TGO grows significantly between the TC and the BC. Based on the ceramic–metal interface morphology shown in Fig. 8, the TGO thickness can be extracted by image processing. Thus, the thickness of TGO that underwent isothermal oxidation and cyclic thermal oxidation can be evaluated, as shown in Fig. 9. The oxidation kinetics equation for the growth of the TGO thickness under isothermal oxidation was established based on the Arrhenius Equation [14],

$$\delta = \{\exp\left[\frac{\Delta H}{R}\left(\frac{1}{T_0}-\frac{1}{T}\right)\right]t\}^n \quad (1)$$

where δ is the thickness of the TGO, t is the oxidation time, T is the absolute temperature for oxidation, R is the uniform gas constant, ΔH is the activation energy, T_0 is the temperature constant and n is the material constant.

For the cyclic oxidation test, the holding time for the specimens in the muffle furnace was 10 min. According to the temperature change with time in the cyclic oxidation tests shown in Fig. 2, the holding time in one thermal cycle can be approximated as 1/6 h. Thus, the TGO thicknesses of specimens in the cyclic thermal oxidation are shown as red circular points in Fig. 9, whereas the results of isothermal oxidation are shown as rectangular points. Based on Eq. (1), the growth laws of the TGO thickness can be fitted by the solid curve shown in Fig. 9.

Comparison between the calculated results and the measured values shows that under the conditions of cyclic oxidation and isothermal

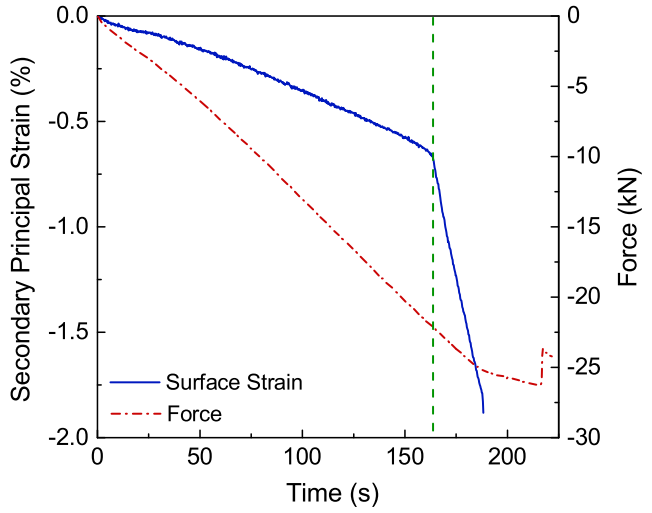

Fig. 6. Evolution of the TBC surface secondary principal strain and compressive force of the testing machine.

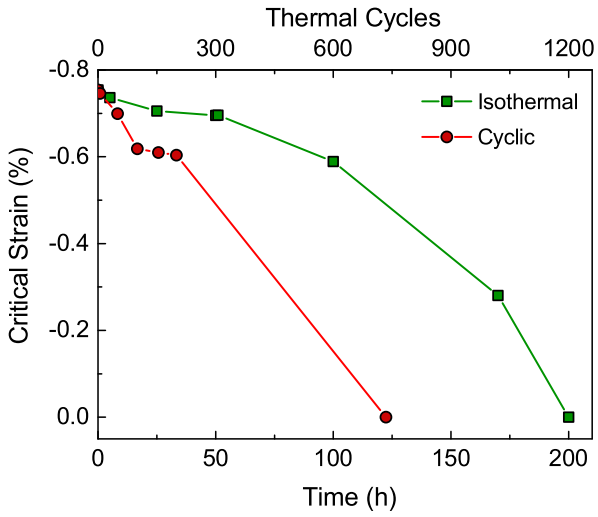

Fig. 7. Evolution of the critical strain.

oxidation, the evolution of TGO thickness with the equivalent holding time is essentially consistent with almost all errors in the range of ±10%, that is, the thermal cycle does not have a significant effect on the growth process of TGO.

4. Interfacial damage in the EB-PVD TBC

4.1. Stress and strain within the TBC system

It is generally considered that the macroscopic spalling of the EB-PVD TBC is caused by the combination of the in-plane compressive stress and the degradation of the ceramic–metal interfacial toughness, which represents the degree of TBC system damage and is closely related to the growth of the TGO and the mechanical behavior of each layer for the TBC system.

The stress and strain within the TBC system under the in-service loadings can be analyzed by establishing a macroscopic finite element model (FEM) [23–27] or by using a simplified macroscopic mechanical model [15,28], in which the former requires the morphology of each layer and the ceramics-metal interface within the TBC system for geometric modeling. Due to the large difference in spatial scale, for

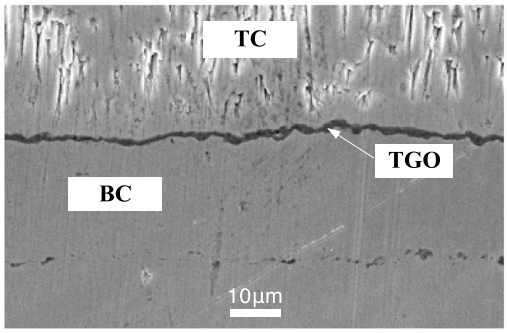

Fig. 8. Typical SEM morphology of the EB-PVD TBC system after the tests.

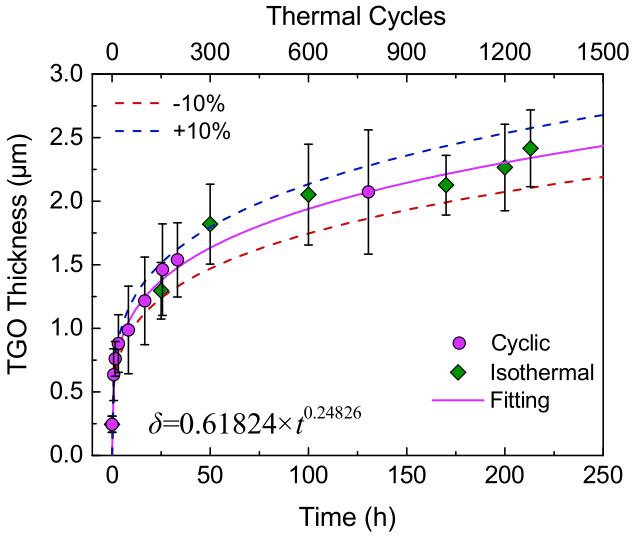

Fig. 9. Evolution of the TGO thickness.

example, the blade substrate size is on the order of centimeters, the thicknesses of the TC and BC are usually tens to hundreds of micrometers, and that of TGO is only a few micrometers. The modeling process is very time consuming and cumbersome, resulting in difficulties in the promotion and application of the TBC FEM method. To facilitate the engineering application, a simplified mechanical model is used to approximately calculate the stress and strain in each layer of the TBC system in this paper.

Since the blade substrate is much more rigid than the TBC system, it can be assumed that the strain of each layer of the TBC can be described on the basis of the strains of the substrate,

$$\varepsilon_i^{\mathrm{tot}} = \varepsilon_i^{\mathrm{th}} + \varepsilon_i^{\mathrm{m}} \approx \varepsilon_s^{\mathrm{tot}} \tag{2}$$

where $\varepsilon_i^{\mathrm{tot}}$, $\varepsilon_i^{\mathrm{th}}$ and $\varepsilon_i^{\mathrm{m}}$ represent the total strain, thermal strain and mechanical strain of the ith layer of the TBC system, respectively, and $\varepsilon_s^{\mathrm{tot}}$ is the total strain of the substrate. The EB-PVD processing temperature T_{pro}, 1000 °C herein, is considered the initial unstressed temperature of the TBC system. When the blade with the TBC system is cooled to room temperature T_0, typically 20 °C, the residual mechanical strain of each layer of the TBC can be calculated as,

$$\varepsilon_i^{\mathrm{m}}(T_0) = \left[\alpha_s(T_{\mathrm{pro}}) - \alpha_i(T_{\mathrm{pro}})\right]\left(T_0 - T_{\mathrm{pro}}\right) \tag{3}$$

where α_s and α_i are the thermal expansion coefficients (TEC) of the substrate and the ith layer of the TBC system, respectively, with a reference temperature of T_0. Then, when the blade is subjected to thermomechanical loading with a temperature T, the total strain and mechanical strain of the substrate can be calculated,

$$\varepsilon_s^{\mathrm{tot}}(T) = \alpha_s(T_{\mathrm{pro}})\left(T_0 - T_{\mathrm{pro}}\right) + \alpha_s(T)\left(T - T_0\right) + \varepsilon_s^{\mathrm{m}}(T), \tag{4}$$

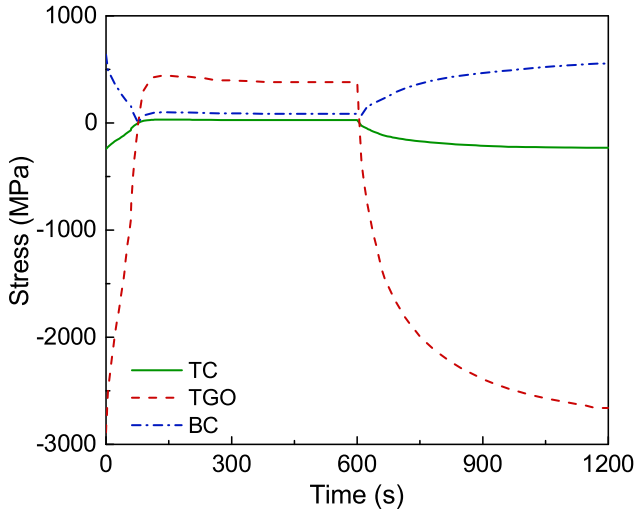

Fig. 10. Evolution of the in-plane stress in each layer constituting the TBC system under a thermal cycle.

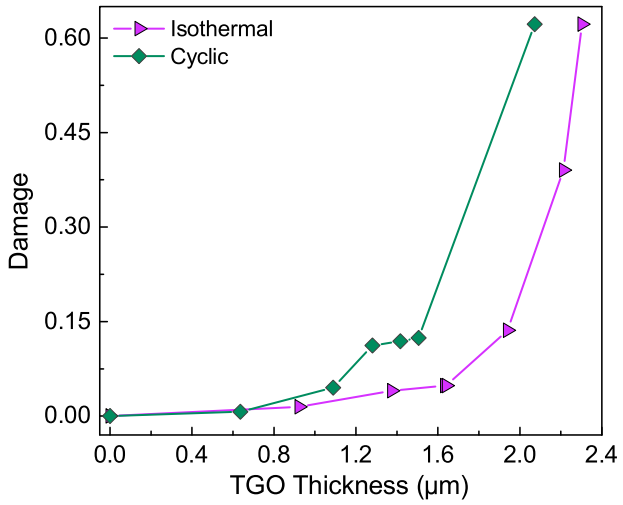

Fig. 11. Evolution of interfacial damage as a function of TGO thickness.

Then, the mechanical strain of each layer of the TBC system is obtained,

$$\varepsilon_i^{\mathrm{m}}(T) = \varepsilon_{\mathrm{s}}^{\mathrm{tot}}(T) - \alpha_i(T_{\mathrm{pro}})\left(T_0 - T_{\mathrm{pro}}\right) - \alpha_i(T)\left(T - T_0\right). \tag{5}$$

Note that the current blade finite element analysis generally uses the reference temperature T_0 at room temperature instead of the TBC process temperature T_{pro} as the unstressed initial temperature. In other words, the total strain of the blade surface obtained by finite element analysis (FEA) is,

$$\widetilde{\varepsilon}_s^{\mathrm{tot}}(T) = \alpha_{\mathrm{s}}(T)\left(T - T_0\right) + \varepsilon_s^{\mathrm{m}}(T). \tag{6}$$

Therefore, when the total surface strain obtained from the blade FEA is used as the constraint of the mechanical analysis of the TBC system it yields,

$$\begin{aligned}\varepsilon_i^{\mathrm{m}}(T) = {} & \widetilde{\varepsilon}_{\mathrm{s}}^{\mathrm{tot}}(T) - \left[\alpha_s(T_{\mathrm{pro}}) - \alpha_i(T_{\mathrm{pro}})\right]\left(T_{\mathrm{pro}} - T_0\right) \\ & - \alpha_i(T)\left(T - T_0\right).\end{aligned} \tag{7}$$

Based on the above method, the in-plane stress evolution of each layer of the TBC system in the typical cyclic thermal oxidation shown in Fig. 2 can be obtained by introducing the plane stress assumption, as shown in Fig. 10. The TC and TGO are subjected to compressive loads at low temperatures, whereas they are subjected to tensile loads at higher temperatures. At room temperature, the residual stress of the TGO is close to −3 GPa, which is essentially consistent with the measured values in [10]. The BC is always subjected to tensile stress during cyclic thermal oxidation, and the tensile stress gradually increases as the temperature decreases.

4.2. Damage characterization

In general, TBC system damage can be characterized through the degradation of the ceramic–metal interface toughness during isothermal oxidation and cyclic oxidation, while the interface toughness can be characterized by the critical compression spalling strain at room temperature [29]. Notably, the effective bearing area of the ceramic–metal interface is reduced due to damage such as microcracks and defects. According to the method mentioned in [13], the equivalent delamination zone is introduced in the TBC system, and the TC is regarded as a circular blister susceptible to buckling. Assuming that the circular blister is subjected to uniform and equivalent biaxial compressive stress, the compressive critical stress equation of the elastic buckling of the constrained circular blister is used to describe the compressive buckling of the TC [30], as described by,

$$\sigma_{\mathrm{c}}^{*} = 1.2235\frac{E_1}{1-\nu_1^2}\left(\frac{h}{r}\right)^2 \tag{8}$$

where σ_{c}^{*} is the absolute value of the critical compressive stress, E_1 and ν_1 are the in-plane elastic modulus and Poisson ratio of the TC, respectively, and r is the initial equivalent radius of the delamination zone. Since the delamination occurs at the ceramic–metal interface, the thickness of the circular plate h is the same as that of the TC. The critical stress decreases as the interface damage increases. The macroscopic damage parameter, D, is introduced into Eq. (8) to obtain,

$$\sigma_{\mathrm{c}}^{*} = 1.2235\frac{E_1}{1-\nu_1^2}\left(\frac{h}{r}\right)^2(1-D) \tag{9}$$

For the initial state, $D = 0$; for complete interface damage, $D = 1$. In fact, with increasing D, the equivalent radius is gradually increased as shown in Eq. (10), and the corresponding area is changed from S_0 to S, as shown in Eq. (10); that is, the damage increases the area of the delamination zone, which is equivalent to a reduction in the bearing capacity of the TBC interface.

$$r = \frac{r_0}{\sqrt{1-D}}, \quad S = \frac{S_0}{1-D}. \tag{10}$$

Substituting the biaxial constitutive relation in the plane stress state into Eq. (9), the damage can be described using the critical strain $\varepsilon_{\mathrm{c}}^{*}$,

$$D = 1 - \frac{1+\nu_1}{1.2235}\left(\frac{r_0}{h}\right)^2\varepsilon_{\mathrm{c}}^{*} \tag{11}$$

where all parameters are the same as in Eq. (10). It is obvious that Eq. (11) realizes the scale conversion from TBC macro failure to interface delamination and damage modeling.

Note that the TBC spalls from the substrate in the compression test at room temperature, and the compressive loads experienced by the TC should include not only the external mechanical strain applied by the testing machine, i.e., the critical strain $\varepsilon_{\mathrm{crit}}$, but also the residual strain obtained by Eq. (3) due to the cooling of the TBC system from the processing temperature to room temperature. Since the DIC measurement is based on the surface state at room temperature, the prestrain ε_0 is not included in the measured value; that is, $\varepsilon_{\mathrm{crit}}$ is actually the strain increment on the TBC surface under mechanical loading. Therefore, the critical strain should be expressed as,

$$\varepsilon_{\mathrm{c}}^{*} = \varepsilon_{\mathrm{crit}} + \varepsilon_0 \tag{12}$$

Then, the damage can be rewritten as,

$$D = 1 - \frac{1+\nu_1}{1.2235}\left(\frac{r_0}{h}\right)^2\left(\varepsilon_{\text{crit}} + \varepsilon_0\right). \tag{13}$$

According to Eq. (13), the damage evolutions of the TBC system with TGO thickness under isothermal oxidation and cyclic oxidation can be obtained, as shown in Fig. 11. At the same TGO thickness, the damage caused by the cyclic oxidation is greater than that by the isothermal oxidation, indicating that cyclic oxidation causes additional damage.

4.3. Damage models

As the TBC interface damage is closely related to the TGO morphological evolution of the ceramic–metal interface, and the difference of the damage caused by the isothermal oxidation and cyclic oxidation has been measured in the tests, it is assumed that the interface damage D is a nonlinear accumulation of oxidative damage D_{ox} and cyclic damage D_{cyc} [13],

$$D = D_{\text{ox}} + D_{\text{cyc}} - D_{\text{ox}} D_{\text{cyc}} \tag{14}$$

where D_{ox} is related to the interface microstructure evolution and can be approximated by the TGO thickness growth, and D_{cyc} is used to describe the additional damage caused by thermal cycling in the cyclic oxidation test, also known as "rumpling damage" [13], which is related to the number of thermal cycles and the TBC mechanical behavior. Besides, there is a minus sign for the damage term $D_{\text{ox}} D_{\text{cyc}}$, considering that the TGO undergoes in-plane compressive stress during cooling process, and the compressive stress will result in displacement instability, which can release elastic strain energy [24], and cause the decrease of the accumulation rate of damage to a certain extent. However, for the BC in MCrAlY materials, the amplitude of rumpling is usually 2–3 times lower than that of the BC in (Ni, Pt)Al materials [31]. In addition, the TBC of the specimens herein did not exhibit significant rumpling after undergoing thermal cycling. Therefore, D_{cyc} is used instead of the rumpling damage, D_{r}, in Courcier's equation [13] to characterize the additional damage caused by thermal cycling. Moreover, because the viscoplastic behavior of the BC material at high temperature is difficult to obtain accurately, the elastic constitutive equation herein is used to describe the evolution of the average in-plane stress and strain of each layer of TBC under thermal mismatch and mechanical loads. The present process can greatly simplify the calculation process to facilitate TBC analysis for complex three-dimensional engineering components despite sacrificing certain precision.

The specimens in the isothermal oxidation experience only one thermal cycle before the compression test at room temperature. When ignoring this thermal cycle, the oxidative damage is an approximate power law with TGO thickness, δ, as shown in Fig. 11. Therefore, the evolution equation of oxidative damage can be established,

$$\mathrm{d}D_{\text{ox}} = \frac{\mathrm{m}}{\delta_0}\left(\frac{\delta}{\delta_0}\right)^{m-1}\mathrm{d}\delta, \tag{15}$$

where δ_0 and m are material constants that can be fitted by the data in interrupted tests for isothermal oxidation. Thus, the evolving relationship between the oxidative damage and the oxidative time also follows an approximate power law according to the Arrhenius formula, and the curve of the damage with the isothermal oxidation time is shown in Fig. 12.

For cyclic oxidation, when the oxidative damage associated with the growth of TGO is removed from the measured damage, the cyclic damage can be approximated by a linear relationship with the number of thermal cycles applied, as shown in Fig. 13. Previous studies have shown that the mechanical behavior of the BC may be the key factor controlling the thermal cycling damage [32]. Therefore, based on the

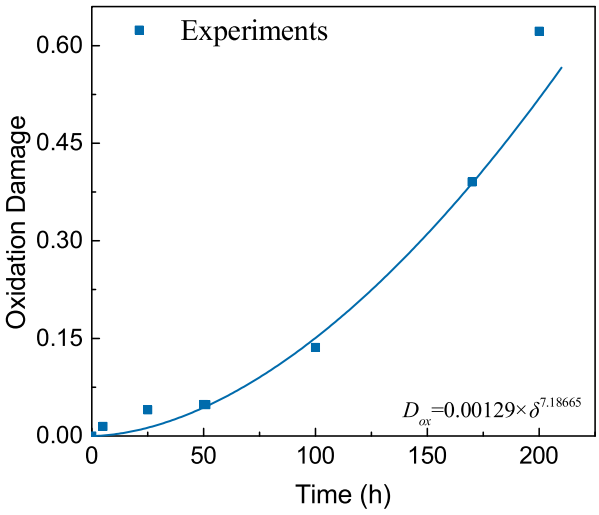

Fig. 12. Evolution of oxidation damage as a function of the isothermal oxidation time.

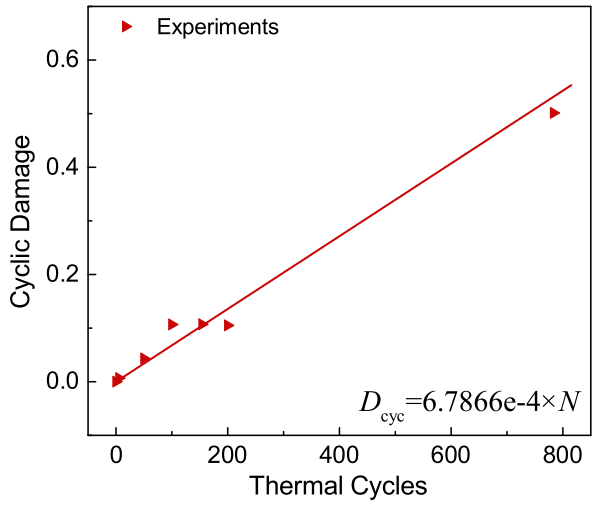

Fig. 13. Evolution of cyclic damage as a function of the number of thermal cycles.

strain fatigue linear accumulation damage model of metal materials, the range of mechanical strain in the BC is used as the damage parameter to establish the damage model of the TBC system,

$$\mathrm{d}D_{\text{cyc}} = \left(\frac{\Delta\varepsilon_{\text{m}}}{\Delta\varepsilon_0}\right)^{c}\mathrm{d}N, \tag{16}$$

where $\Delta\varepsilon_{\text{m}}$ is the mechanical strain range in the BC corresponding to each thermal cycle, which it can be calculated by using the simplified mechanical model mentioned above; $\Delta\varepsilon_0$ and c are material constants, which can be fitted by data obtained from the spontaneously spalling specimens in the cyclic oxidation test. Thus, the curve of the cyclic damage for the number of oxidation cycles is shown in Fig. 13.

Finally, the total damage of the isothermal oxidation and cyclic oxidation tests can be obtained, as shown in Fig. 14. The errors between the calculated value and the measured value are less than ±10%.

5. Conclusions

The durability evaluation of the EB-PVD TBC system is one of the key difficulties in engineering applications. The interfacial toughness degradation of the TBC system undergoing isothermal oxidation and cyclic oxidation was investigated through compression tests at room

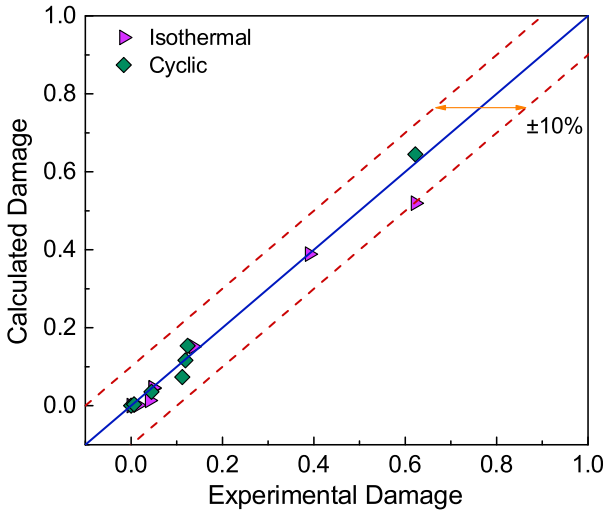

Fig. 14. Prediction of total damage in the isothermal oxidation and cyclic oxidation tests.

temperature with hourglass specimens in the single-crystal superalloy substrate based on the DIC method in this paper. The following conclusions can be drawn:

- Based on the noncontact measurement method, it is clearly determined that the delamination of the TBC causes a sudden change in the second principal strain slope of the surface stress concentration region, while the single-crystal substrate has not yet entered the plastic region. Therefore, the maximum compressive strain in the stress concentration region at the TBC spalling moment can be accurately identified as the criterion for the initiation of TBC spalling, and the evolution relationship of the critical compressive strain of the TBC with the oxidation time is established.
- The thickness growth of the TGO follows an approximate power law with oxidation time. The evolution of the TGO thickness obtained using the equivalent holding time for the cyclic thermal oxidation is essentially the same as that of isothermal oxidation. The Arrhenius formula is used to establish the oxidation kinetics equation of TGO thickness growth, in which the errors of prediction lie within ±10%.
- The interface damage of TBCs is characterized by the degradation of the critical strain at room temperature relative to the processes status of TBCs, considering the influence of the residual stress in TC. Based on the simplified mechanical model of the TBC system, the residual stress calculated in TGO is very close to the measured data in the literature, demonstrating the engineering applicability of the simplified mechanical model for avoiding the complexity of finite element modeling caused by the large difference in spatial scale between the TBC and the blade substrate.
- The critical compressive strain of the TBC decreases with an increasing oxidation time and number of thermal cycles, indicating that the interface toughness and load-carrying capacity of the TBC system is gradually reduced and that isothermal oxidation and cyclic oxidation cause obvious damage accumulation. The damage caused by isothermal oxidation approximately follows a power law with the increasing thickness of the TGO. At the same TGO thickness, the damage caused by the cyclic oxidation is greater than that of the isothermal oxidation, indicating that the thermal cycling causes additional cyclic damage, and the cyclic damage is approximately linear with the number of thermal cycles.
- The life model based on the nonlinear accumulation of the cyclic damage and the oxidative damage can accurately predict the spalling life of the TBC system. The errors between the damage prediction result and the measured value of the isothermal oxidation and cyclic oxidation test are within 10%.

Declaration of competing interest

The authors declare that they have no known competing financial interests or personal relationships that could have appeared to influence the work reported in this paper.

CRediT authorship contribution statement

Fulei Jing: Investigation, Writing - original draft. **Junjie Yang:** Conceptualization, Formal analysis, Funding acquisition, Methodology, Project administration, Resources, Software, Supervision. **Zhengmao Yang:** Conceptualization, Data curation, Methodology, Project administration, Writing - review & editing. **Wu Zeng:** Validation, Visualization.

Acknowledgment

The present work is financed by the China Natural Science Foundation under the contract numbers 51905510.

References

[1] R. Kromer, F. Mauget, L. Despres, S. Costil, J. Cormier, Thermo-mechanical fatigue evaluation of a thermal barrier coating bond-coatless system, Mater. Sci. Eng. A 756 (2019) 130–141.
[2] Chungen Zhou, Na Wang, Huibin Xu, Comparison of thermal cycling behavior of plasma-sprayed nanostructured and traditional thermal barrier coatings, Mater. Sci. Eng. A 452–453 (2007) 569–574.
[3] G.W. Goward, Progress in coatings for gas turbine airfoils, Surf. Coat. Technol. 108–109 (1998) 73–79.
[4] L. Saucedo-Mora, K. Slámečka, U. Thandavamoorthy, T.J. Marrow, Multi-scale modeling of damage development in a thermal barrier coating, Surf. Coat. Technol. 276 (2015) 399–407.
[5] Robert Vaßen, Maria Ophelia Jarligo, Tanja Steinke, Daniel Emil Mack, Detlev Stöver, Overview on advanced thermal barrier coatings, Surf. Coat. Technol. 205 (4) (2010) 938–942.
[6] R. Ragupathy, R.K. Mishra, R.D. Misal, Life estimation of tbc on an aero gas turbine combustor: A finite element approach, in: ASME 2011 Turbo Expo: Turbine Technical Conference and Exposition, Vol. Volume 5: Heat Transfer, Parts A and B, pp. 2037–2043.
[7] V.K. Tolpygo, D.R. Clarke, K.S. Murphy, Oxidation-induced failure of EB-PVD thermal barrier coatings, Surf. Coat. Technol. 146–147 (2001) 124–131.
[8] Tom Strangman, Derek Raybould, Ahsan Jameel, Wil Baker, Damage mechanisms, life prediction, and development of EB-PVD thermal barrier coatings for turbine airfoils, Surf. Coat. Technol. 202 (4) (2007) 658–664.
[9] A.G. Evans, D.R. Clarke, C.G. Levi, The influence of oxides on the performance of advanced gas turbines, J. Eur. Ceram. Soc. 28 (7) (2008) 1405–1419.
[10] A.G. Evans, D.R. Mumm, J.W. Hutchinson, G.H. Meier, F.S. Pettit, Mechanisms controlling the durability of thermal barrier coatings, Prog. Mater. Sci. 46 (5) (2001) 505–553.
[11] N.M. Yanar, F.S. Pettit, G.H. Meier, Failure characteristics during cyclic oxidation of yttria stabilized zirconia thermal barrier coatings deposited via electron beam physical vapor deposition on platinum aluminide and on NiCoCrAlY bond coats with processing modifications for improved performances, Metall. Mater. Trans. A 37 (5) (2006) 1563–1580.
[12] C. Bargraser, P. Mohan, K. Lee, B. Yang, J. Suk, S. Choe, Y.H. Sohn, Life approximation of thermal barrier coatings via quantitative microstructural analysis, Mater. Sci. Eng. A 549 (2012) 76–81.
[13] C. Courcier, V. Maurel, L. Rmy, S. Quilici, I. Rouzou, A. Phelippeau, Interfacial damage based life model for EB-PVD thermal barrier coating, Surf. Coat. Technol. 205 (13) (2011) 3763–3773.
[14] R.A. Miller, Progress toward life modeling of thermal barrier coatings for aircraft gas turbine engines, J. Eng. Gas Turbines Power 109 (4) (1987) 448–451.
[15] C. Rinaldi, L. De Maria, M. Mandelli, Assessment of the spent life fraction of gas turbine blades by coating life modeling and photostimulated luminescence piezospectroscopy, J. Eng. Gas Turbines Power 132 (11) (2010).
[16] Y.Y. Zhang, H.X. Deng, H.J. Shi, H.C. Yu, B. Zhong, Failure characteristics and life prediction for thermally cycled thermal barrier coatings, Surf. Coat. Technol. 206 (11) (2012) 2977–2985.
[17] L. Rémy, C. Guerre, I. Rouzou, R. Molins, Assessment of TBC oxidation-induced degradation using compression tests, Oxid. Met. 81 (1) (2014) 3–15.

[18] Bing Pan, Digital image correlation for surface deformation measurement: historical developments, recent advances and future goals, Meas. Sci. Technol. 29 (8) (2018) 082001.
[19] Zhengmao Yang, Huang Yuan, Hui Liu, Evolution and characterization of cyclic thermal shock-induced thermomechanical damage in oxide/oxide ceramics matrix composites, Int. J. Fatigue 120 (2019) 150–161.
[20] Zhengmao Yang, Junjie Yang, Investigation of long-term thermal aging-induced damage in oxide/oxide ceramic matrix composites, J. Eur. Ceram. Soc. (2019).
[21] Zhengmao Yang, Hui Liu, Effects of thermal aging on the cyclic thermal shock behavior of oxide/oxide ceramic matrix composites, Mater. Sci. Eng. A 769 (2020) 138494.
[22] V. Maurel, P. de Bodman, L. Rémy, Influence of substrate strain anisotropy in TBC system failure, Surf. Coat. Technol. 206 (7) (2011) 1634–1639.
[23] E.P. Busso, J. Lin, S. Sakurai, M. Nakayama, A mechanistic study of oxidation-induced degradation in a plasma-sprayed thermal barrier coating system.: Part I: model formulation, Acta Mater. 49 (9) (2001) 1515–1528.
[24] A.M. Karlsson, C.G. Levi, A.G. Evans, A model study of displacement instabilities during cyclic oxidation, Acta Mater. 50 (6) (2002) 1263–1273.
[25] M. Caliez, F. Feyel, S. Kruch, J.L. Chaboche, Oxidation induced stress fields in an EB-PVD thermal barrier coating, Surf. Coat. Technol. 157 (2) (2002) 103–110.
[26] U. Hermosilla, M.S.A. Karunaratne, I.A. Jones, T.H. Hyde, R.C. Thomson, Modelling the high temperature behaviour of TBCs using sequentially coupled microstructuralcmechanical FE analyses, Mater. Sci. Eng. A 513–514 (2009) 302–310.
[27] W. Zhu, Z.B. Zhang, L. Yang, Y.C. Zhou, Y.G. Wei, Spallation of thermal barrier coatings with real thermally grown oxide morphology under thermal stress, Mater. Des. 146 (2018) 180–193.
[28] M. Harvey, C. Courcier, V. Maurel, L. Rmy, Oxide and TBC spallation in β-nial coated systems under mechanical loading, Surf. Coat. Technol. 203 (5) (2008) 432–436.
[29] X. Zhao, J. Liu, D.S. Rickerby, R.J. Jones, P. Xiao, Evolution of interfacial toughness of a thermal barrier system with a pt-diffused γ/γ' bond coat, Acta Mater. 59 (16) (2011) 6401–6411.
[30] J.W. Hutchinson, Z. Suo, Mixed mode cracking in layered materials, in: John W. Hutchinson, Theodore Y. Wu (Eds.), Advances in Applied Mechanics, Vol. 29, Elsevier, 1991, pp. 63–191.
[31] Y. Chen, X. Zhao, M. Bai, L. Yang, C. Li, L. Wang, J.A. Carr, P. Xiao, A mechanistic understanding on rumpling of a NiCoCrAlY bond coat for thermal barrier coating applications, Acta Mater. 128 (2017) 31–42.
[32] D.S. Balint, J.W. Hutchinson, An analytical model of rumpling in thermal barrier coatings, J. Mech. Phys. Solids 53 (4) (2005) 949–973.